This is a preprint, the final version is subject to change, of the American Mineralogist (MSA)
Cite as Authors (Year) Title. American Mineralogist, in press.
(DOI will not work until issue is live.) DOI: http://dx.doi.org/10.2138/am-2017-5917

Revision 3

The spin state of Fe^{3+} in lower mantle bridgmanite

Ryosuke Sinmyo*, Catherine McCammon, Leonid Dubrovinsky

Bayerisches Geoinstitut, Universitaet Bayreuth, D-95440 Bayreuth, Germany

*Corresponding author. (E-mail: ryosuke.sinmyo@elsi.jp) Now at Earth-Life Science Institute, Tokyo Institute of Technology

Abstract

Iron- and aluminum-bearing $MgSiO_3$ bridgmanite is the most abundant mineral in the Earth's interior; hence its crystal chemistry is fundamental to expanding our knowledge of the deep Earth and its evolution. In this study, the valence and spin state of iron in well characterized Al-free Fe^{3+}-rich bridgmanite were investigated by means of Mössbauer spectroscopy to understand the effect of ferric iron on the spin state. We found that a minor amount of Fe^{3+} is in the low spin state above 36 GPa and that its proportion does not increase substantially with pressure up to 83 GPa. This observation is consistent with recent experimental studies that used Mössbauer and X-ray emission spectroscopy. In the Earth's deep lower mantle, Fe^{3+} spin crossover may take place at depths below 900 and 1200 km in pyrolite and MORB, respectively. However, the effect of spin crossover on physical properties may be small due to the limited amount

19 of Fe^{3+} in the low spin state.

20

21 **Introduction**

22 The crystal chemistry of terrestrial minerals is fundamental to understanding
23 the Earth's interior and its evolution. Iron- and aluminum-bearing $MgSiO_3$ bridgmanite
24 (Bdg) is the most abundant mineral in the Earth's interior and contains a substantial (up
25 to about 20 at. %) amount of iron, which is the fourth most abundant element in the
26 mantle. Bdg can incorporate a substantial amount of Fe^{3+} (e.g., McCammon 1997; Frost
27 et al. 2004), while olivine, the dominant mineral in the upper mantle, accommodates
28 essentially no Fe^{3+} (e.g., McCammon 2005). The substitution of Fe^{3+} for Fe^{2+} has a
29 large influence on physical and chemical properties of Bdg such as elastic constants,
30 iron partition coefficients and electrical/thermal conductivity (Ohta et al. 2010; 2014;
31 Boffa Ballaran et al. 2012; Sinmyo and Hirose 2013; Sinmyo et al. 2014a; Wolf et al.
32 2015; Yoshino et al. 2016). Moreover, both experiments and theoretical calculations
33 suggest that iron in Bdg undergoes spin crossover under deep mantle conditions (Badro
34 et al. 2004; Lin et al. 2012; Potapkin et al. 2013; Mashino et al. 2014). Although iron
35 spin crossover can strongly influence the physical properties of lower mantle minerals,
36 e.g., elastic constants and thermal/electrical conductivity (Lundin et al. 2008; Keppler et

al. 2008; Ohta et al. 2010; Catalli et al. 2011), the pressure of spin crossover in Bdg is not well constrained (see reviews by Lin et al. 2013; McCammon et al. 2013 and references therein). Challenges arise due mainly to the presence of iron in two different valence states (Fe^{2+} and Fe^{3+}), and two different sites in the perovskite structure (8-12 coordinated A-site and octahedral B-site). Fe^{2+}, which is observed to occupy the A-site, undergoes spin crossover from high spin to intermediate spin (McCammon et al. 2008; Lin et al. 2008; Potapkin et al. 2013), although theoretical calculations do not support the existence of the intermediate spin state of Fe^{2+} (Hsu et al. 2011; Metsue and Tsuchiya 2012). There is general consensus that Fe^{3+} remains in the high spin state to at least 100 GPa when it occupies the A-site (Catalli et al. 2010, 2011; Fujino et al. 2012; Lin et al. 2012; Potapkin et al. 2013; Glazyrin et al. 2014; Kupenko et al. 2014), but undergoes spin crossover from high spin to low spin at 20~60 GPa when it occupies the B-site (Catalli et al. 2010; 2011; Fujino et al. 2012; Lin et al. 2012; Kupenko et al. 2015). These observations strongly suggest that the spin crossover pressure is dominantly controlled by Fe^{3+} in the B-site. It has been reported that Fe^{3+} occupies the A-site of Bdg regardless of the oxidation state concentration, Al content and pressure (Kudoh et al. 1990; Vanpeteghem et al. 2006; Glazyrin et al. 2014), while some recent studies have reported that Al-free and Fe^{3+}-bearing Bdg accommodate a detectable

55 amount of Fe^{3+} in the B-site (Catalli et al. 2011; Lin et al. 2012; Hummer and Fei 2012;
56 Kupenko et al. 2015). Since previous studies have investigated Bdg with a limited
57 amount of Fe^{3+}, the electronic state of Fe^{3+} is not well understood, even though the
58 electronic state of iron in Al-free Fe^{3+}-rich Bdg may have a significant effect on the
59 physical/chemical properties of subducted depleted lithospheric mantle with
60 harzburgitic bulk composition (Ringwood 1991). Furthermore, it is recognized that
61 sample synthesis in the diamond anvil cell by laser heating may cause heterogeneity in
62 chemical composition and/or redox state of the sample (e.g., Fialin et al. 2008; Sinmyo
63 and Hirose 2010). Therefore, to minimize the experimental uncertainty, the $Fe^{3+}/\Sigma Fe$
64 ratio of samples pre-synthesized using a large volume press should be characterized
65 before the sample is compressed with a diamond anvil cell. Here, our study aims to
66 explore the spin state of iron under lower mantle conditions by investigating the rarely
67 studied, but well defined Al-free Fe^{3+}-rich Bdg, which provides insight into the complex
68 effects of Al^{3+} and Fe^{3+} on the spin state.
69

70 **Experimental procedure**

71 The sample was synthesized using a multi anvil apparatus. A mixture of fine
72 grained SiO_2 [55.23 wt %] + MgO [37.05 wt %] + $^{57}Fe_2O_3$ (90% enriched) [7.72 wt %]

was ground well for about one hour, and then dried at 1273 K in a furnace for one day. We used Fe_2O_3 as a starting material to maximize Fe^{3+} content in the sample. The final mix was loaded into a gold capsule and then packed into a MgO container. The multi-anvil synthesis used $LaCrO_3$ for the heater, and was run for 45 minutes at pressure and temperature conditions of 26 GPa and 1973 K, respectively. The synthesized sample was examined using a field-emission-type scanning electron microscope (SEM) (Leo Gemini 1530) and the chemical composition was determined using an electron microprobe (JEOL JXA-8200) operated at 15 kV and 15 nA. Phase identification was performed by powder X-ray diffraction (XRD) using a FR-D high-brilliance Rigaku X-ray diffractometer with Mo-Kα radiation operated at 55 kV and 60 mA.

The high-pressure Mössbauer spectroscopic study was conducted using a diamond anvil cell. Diamonds with 250 μm diameter culets were used as anvils. The polycrystalline sample from the multianvil synthesis was loaded into a hole drilled in a rhenium gasket. Mössbauer spectroscopy was conducted using a nominal 370 MBq ^{57}Co high specific activity source in a rhodium matrix. The velocity scale was calibrated relative to ^{57}Fe foil. Mössbauer spectra were analyzed using the MossA software package (Prescher et al. 2012). Mössbauer spectra were collected with increasing pressure up to 83 GPa, and then the pressure was gradually decreased toward ambient

conditions.

Results

The sample synthesized using the multianvil press was characterized by XRD, Mössbauer spectroscopy and electron microprobe analysis. The electron microprobe analysis yielded a chemical composition of $Mg_{0.971(11)}Fe_{0.064(4)}Si_{0.979(7)}O_3$. The grain size was around 50 μm in diameter. Although a trace amount of quenched liquid material was observed at the very edge of the sample, it was easily removed from the capsule before selecting the Bdg sample for diamond anvil cell experiments. Most likely due to the partitioning of iron between liquid and Bdg, the iron content in the Bdg was depleted in comparison to the starting material. XRD measurements showed that the obtained sample was a single phase of Bdg. The $Fe^{3+}/\Sigma Fe$ ratio of the perovskite was determined to be 0.53(6) according to Mössbauer measurements at ambient conditions. Based on this result, the chemical composition can be described as $Mg_{0.971}Fe^{2+}_{0.030}Fe^{3+}_{0.034}Si_{0.979}O_3$. The total charge of the cations slightly exceeds six (6.02), which may be due to vacancies in the crystal lattice (Hummer and Fei 2012). A quantitative discussion is not possible, however, since the excess amount (+ 0.3 %) is smaller than the uncertainty in the measurements (~ 1 %).

Mössbauer spectra were collected up to 83 GPa at 15 pressure points in total (Fig. 1). The pressure variation of the obtained hyperfine parameters center shift (CS) and quadrupole splitting (QS) are summarized in Figure 2 and Table 1. The spectra at ambient conditions are composed of two components corresponding to Fe^{2+} with higher CS and QS values (hereafter Fe^{2+} #1) and Fe^{3+} with lower CS and QS values (Fe^{3+} #1). The QS values of Fe^{2+} #1 and Fe^{3+} #1 slightly increase with increasing pressure, while their CS values are almost constant (Fig. 2). Above 12 GPa, we observed a component with a high QS value (Fe^{2+} #2), which corresponds to Fe^{2+} in the distorted A-site of Bdg (McCammon et al. 2008; Kupenko et al. 2014). The abundance of Fe^{2+} #2 does not change substantially from 12 to 83 GPa (Fig. 3). At higher pressure, an additional component was observed above 36 GPa (Fe^{3+} #2). This new component exhibits almost zero CS and QS similar to the value for Fe^{3+} #1. These hyperfine parameters are comparable to those of the Fe^{3+} component found in Al, Fe-bearing Bdg at around 40 GPa after laser heating (Kupenko et al. 2015). As in the case of the Fe^{2+} #1 and Fe^{3+} #1 components, the QS values of Fe^{2+} #2 and Fe^{3+} #2 slightly increase with pressure, in contrast to the constant CS value (Fig. 2). Parallel to the slight increase in abundance of Fe^{3+} #2 with increasing pressure from 40 to 53 GPa, the abundance of Fe^{3+} #1 decreases to compensate, maintaining an essentially constant amount of Fe^{3+} (Fig. 3). The

hyperfine parameters vary with pressure in a highly consistent way during compression and decompression (Fig. 2), and the $Fe^{3+}/\Sigma Fe$ ratio refined independently at each data point remains nearly constant throughout the experiment (Fig. 3).

Discussion

Fe^{3+} in Al-free Bdg

It is well known that the $Fe^{3+}/\Sigma Fe$ ratio in Al-bearing Bdg is remarkably high (about 0.5) even under low oxygen fugacity conditions (e.g., McCammon 2005). The high $Fe^{3+}/\Sigma Fe$ ratio can be explained by a coupled substitution mechanism involving Fe^{3+}-Al to Mg-Si in Bdg (Frost et al. 2004; McCammon et al. 2004). In this study, the $Fe^{3+}/\Sigma Fe$ ratio was about 0.5 in the Al-free Bdg synthesized from Fe^{3+}-rich starting material, which is considerably higher than that for Al-free Bdg synthesized from Fe^{2+}-dominant material (Frost et al. 2004 McCammon et al. 2004; Sinmyo et al. 2008). This observation suggests that $Fe^{3+}/\Sigma Fe$ of Al-free Bdg depends on oxygen fugacity as suggested by McCammon et al. (2004). Indeed, Hummer and Fei (2012) and Mashino et al. (2014) reported a $Fe^{3+}/\Sigma Fe$ ratio close to one in Bdg synthesized from Fe^{3+}-rich material. Fe^{3+} #1 most likely occupies the A-site of Bdg because ferric iron mostly occupies the A-site of Bdg at ambient conditions when the ferric iron concentration is <

145 0.04 per formula unit (Hummer and Fei 2012; Sinmyo et al. 2014b). The Fe^{3+} #2
146 component shows moderate QS ~ 1 and low CS ~ 0 (Table 1). These values are
147 consistent with low spin Fe^{3+} in the octahedral sites of the high-pressure phase of
148 FeOOH (Xu et al. 2013), $CaFe_2O_4$ (Greenberg et al. 2013), rare earth orthoferrites with
149 the perovskite structure (Rozenberg et al. 2005), and Al,Fe-bearing Bdg (Kupenko et al.
150 2015). This observation strongly supports the theoretical work of Hsu et al. (2011), who
151 suggested that Fe^{3+} is in the low-spin state in the B-site of Bdg.

152 Pioneering work by Fujino et al. (2012) reported that an equilibrium site
153 distribution of iron may be difficult to achieve, even with annealing by laser heating.
154 However, more recent work showed that the site distribution does not change
155 substantially before and after annealing (Glazyrin et al. 2014; Kupenko et al. 2015; Lin
156 et al. 2016). Also, *in situ* single crystal XRD measurements at high pressure
157 demonstrated that the site occupancy of iron did not change remarkably before, during
158 and after laser heating (Glazyrin et al. 2014). Lin et al. (2016) also showed that the site
159 distribution does not change after annealing, although X-ray emission spectra became
160 sharp after heating. Generally, annealing is important to achieving equilibrium; however
161 at the same time laser heating may cause undesired chemical heterogeneity in the
162 sample (e.g., Sinmyo and Hirose 2010), which can lead to a large uncertainty in

property measurements. For more detailed knowledge in the future, it is necessary to develop a heating technique with smaller temperature gradient in the sample, such as externally/internally resistive heating.

It is notable that independent studies agree that Fe^{3+} mainly occupies the A-site of Al-free Bdg with moderate Fe^{3+} content (< 0.04 per formula unit) (Lin et al. 2012; Sinmyo et al., 2014b; this study) for samples synthesized at ~25 GPa in a large volume press. Our current results strongly support a small amount of Fe^{3+} distributed onto the B-site of Bdg under pressure. This suggests that A-site of Bdg is more compressible than the B-site, although it should be examined by a future study.

Fe^{3+} in the low-spin state

The new component observed above 36 GPa (Fe^{3+} #2) can be assigned to low spin Fe^{3+} in the B site based on hyperfine parameters reported by Kupenko et al. (2015). Fe^{3+} may have been in the low-spin state when it was distributed onto the B-site of bridgmanite as reported by Kupenko et al. (2015). This inference is consistent with theoretical predictions (e.g., Hsu et al. 2011). Our results show that Fe^{3+} in the low-spin state never exceeds ~18 % of total iron (Fig. 3). This value corresponds to 0.01 cations per formula unit of Fe in the low-spin state in the chemical formula $Mg_{0.971}Fe_{0.064}Si_{0.979}O_3$. Such a minor amount of low-spin iron is consistent with recent

181 experimental studies (Fujino et al. 2012; Lin et al. 2012; Kupenko et al. 2015). It is
182 known that spin crossover can induce pronounced anomalies in the compressibility of
183 minerals (e.g., Fei et al. 2007; Bykova et al. 2016). However, such an anomaly in Bdg
184 compression has hardly been observed, even with single crystal XRD measurements
185 using a soft pressure medium (Boffa Ballaran et al. 2012; Mao et al. 2015). This
186 behavior is possibly due to the limited amount of ferric iron undergoing spin crossover
187 at high pressure. Caracas et al. (2014) showed that spin crossover can be detected by
188 fine analysis of XRD patterns collected for iron-rich $Mg_{0.5}Fe_{0.5}SiO_3$ Bdg. Although
189 Mössbauer spectroscopy is sensitive to the electronic state of iron, a minor amount of
190 Fe^{3+} may not be recognized during analysis of a Fe^{2+}-rich sample. Previous
191 disagreement among studies using XRD, Mössbauer, and X-ray emission spectroscopy
192 (XES) can be explained by the low amount of low-spin Fe^{3+}. Notably, the obtained
193 proportion of low-spin Fe^{3+} is consistent between XES measurements (Fujino et al.
194 2012) and Mössbauer spectroscopy results (Lin et al. 2012; Kupenko et al. 2015; this
195 study) for Bdg synthesized in the multi-anvil press.

196 Figure 4 summarizes the CS and QS values obtained in this study. Fe^{2+} #1 is
197 high spin Fe^{2+} in the A-site (e.g., McCammon et al. 2013). Based on the hyperfine
198 parameters, Fe^{2+} #2 is intermediate spin Fe^{2+} in the A-site (McCammon et al. 2008), or

high-spin Fe^{2+} in the A-site with a high QS value (Hsu et al. 2010). CS and QS values of Fe^{3+} #1 are generally similar to Fe^{3+} in the A-site of Al-free Bdg reported at ambient conditions ("M2" and "M3" components in Hummer and Fei 2012). Hyperfine parameters of Fe^{3+} #2 are similar to those for low-spin Fe^{3+} reported in a previous study of Bdg (Kupenko et al. 2015). We note that all of the data by Hummer and Fei (2012) were measured at ambient conditions. It is thus likely that all iron in their study is in the high-spin state, while in our high-pressure study we suggest that the Fe^{3+} #2 component is in the low-spin state. Moreover, the parameters are also quite similar to recently observed values for low-spin Fe^{3+} in Fe_2O_3 at high pressure (Bykova et al. 2016). Theoretical calculations predicted a high QS value (about 2-3 mm/s) for low-spin Fe^{3+} in Bdg (e.g., Hsu et al. 2011). However, our results in relation to Fe^{3+} in Bdg do not show a QS value higher than 1.5 mm/s regardless of the pressure, consistent with results of Lin et al. (2012) and Kupenko et al. (2015). Although the source of this inconsistency is unclear, the results of theoretical calculations may be affected by iron concentration and structural/magnetic configuration (Umemoto et al. 2008).

Implications

Figure 5 summarizes the relation between the concentration of Fe^{3+} and the pressure at which the fraction of low-spin iron is saturated in Bdg. We have fitted the

217 saturation pressure empirically as a function of Fe^{3+} content using an exponential curve.
218 We used data for Bdg synthesized using a large volume press and with known $Fe^{3+}/\Sigma Fe$
219 ratio (Jackson et al. 2005; Li et al. 2006; Fujino et al. 2012; Lin et al. 2012; Kupenko et
220 al. 2015). As the Fe^{3+} content increases, the pressure of saturation increases (Fig. 5).
221 This behavior is similar to the previously reported relation between Fe^{2+} content and
222 spin-crossover pressure in $(Mg,Fe^{2+})O$ ferropericlase (Fei et al. 2007; Yoshino et al.
223 2011). Such a similarity may be due to the general relation between the spin state of
224 iron and the lattice volume altered by the impurity. The amount of Fe^{3+} in the deep
225 Earth depends on the bulk composition of the rock assemblage in the lower mantle,
226 since it is sensitive to Al content and bulk iron content (Nakajima et al. 2012). The
227 concentration of Fe^{3+} in Bdg is reported to be 0.01 - 0.04, 0.04 - 0.06 and 0.15 - 0.30
228 cations pfu in the harzburgite, pyrolite and MORB bulk compositions, respectively
229 (Sinmyo et al. 2011; Nakajima et al. 2012). Spin crossover of Fe^{3+} may take place at a
230 depth of about 900 km (35 GPa) in pyrolite and 1200 km (50 GPa) in MORB
231 composition according to this study (Fig. 5). It should be deeper in the hotter mantle,
232 since the spin crossover occurs at a higher and wider pressure range at high temperature
233 (Wentzcovitch et al. 2009; Wang et al. 2015). Boffa Ballaran et al. (2012) and Mao et al.
234 (2015) suggested that the elastic properties of Bdg are not substantially altered by iron

235 spin crossover. Moreover, as shown in this study, low-spin Fe^{3+} is a minor component
236 throughout the lower mantle; thus the effect on elasticity is not likely to be visible in
237 seismic observations. However, since electrical conductivity is sensitive to the spin state
238 (Ohta et al. 2010; Yoshino et al. 2011), spin crossover may be detected in geomagnetic
239 observations. Additionally, even though the amount of low-spin Fe^{3+} may be small, spin
240 crossover can have a non-negligible effect on the partition coefficient of iron between
241 Bdg and ferropericlase (e.g., Lin et al., 2013), which can strongly influence the structure
242 and dynamics of the lower mantle. The plot shown in Fig. 5 suggests that spin crossover
243 in Fe^{3+} may take place at a depth of about 900 and 1200 km in pyrolite an MORB
244 composition, respectively. Electrical conductivity and the iron partition coefficient
245 could change at such depths due to spin crossover, although available data are currently
246 limited to Fe^{3+}-bearing bulk compositions such as pyrolite (Ohta et al. 2010; Irifune et
247 al. 2010; Sinmyo and Hirose 2013; Prescher et al. 2014). Recent studies have reported
248 that the redox state of the Earth's mantle may be more heterogeneous than previously
249 thought (Frost and McCammon 2008; Stagno et al., 2013; Kaminsky et al., 2015).
250 Nakajima et al. (2012) showed that the Fe^{3+} content is 0.02 per formula unit higher in
251 Bdg synthesized in a rhenium capsule compared to a diamond capsule. This implies that
252 the spin crossover pressure may differ by ~10 GPa between the rhenium-rhenium oxide

253 buffer and the CCO buffer, since the crossover pressure significantly increases with
254 increasing Fe^{3+} content in Bdg (Fig. 5). Redox heterogeneities may be detectable by
255 precise magnetotelluric measurements at lower mantle depths.

256

257 **Acknowledgments**

258 R.S. was supported by a Research Fellowship for Postdoctoral Researchers awarded by
259 the Alexander von Humboldt Foundation. We appreciate the constructive review
260 comments of two anonymous reviewers and the editor.

261

262 **References cited**

263 Badro, J., Rueff, J.P., Vanko, G., Monaco, G., Fiquet, G., and Guyot, F. (2004)
264 Electronic transitions in perovskite: Possible nonconvecting layers in the lower
265 mantle. Science, 305(5682), 383-386.
266 Boffa Ballaran, T., Kurnosov, A., Glazyrin, K., Frost, D.J., Merlini, M., Hanfland, M.,
267 and Caracas, R. (2012) Effect of chemistry on the compressibility of silicate
268 perovskite in the lower mantle. Earth and Planetary Science Letters, 333,
269 181-190.
270 Bykova, E., Dubrovinsky, L., Dubrovinskaia, N., Bykov, M., McCammon, C.,

271 Ovsyannikov, S.V., Liermann, H.P., Kupenko, I., Chumakov, A.I., Rüffer, R.,
272 Hanfland, M., and Prakapenka, V. (2016) Structural complexity of simple Fe_2O_3
273 at high pressures and temperatures. Nature Communications, 7:10661, doi:
274 10.1038/ncomms10661.
275 Caracas, R., Ozawa, H., Hirose, K., Ishii, H., Hiraoka, N., Ohishi, Y., and Hirao, N.
276 (2014) Identifying the spin transition in Fe^{2+}-rich $MgSiO_3$ perovskite from X-ray
277 diffraction and vibrational spectroscopy. American Mineralogist, 99(7),
278 1270-1276.
279 Catalli, K., Shim, S.-H., Prakapenka, V.B., Zhao, J., Sturhahn, W., Chow, P., Xiao, Y.,
280 Liu, H., Cynn, H., and Evans, W.J. (2010) Spin state of ferric iron in $MgSiO_3$
281 perovskite and its effect on elastic properties. Earth and Planetary Science
282 Letters, 289(1-2), 68-75.
283 Catalli, K., Shim, S.-H., Dera, P., Prakapenka, V.B., Zhao, J., Sturhahn, W., Chow, P.,
284 Xiao, Y., Cynn, H., and Evans, W.J. (2011) Effects of the Fe^{3+} spin transition on
285 the properties of aluminous perovskite-New insights for lower-mantle seismic
286 heterogeneities. Earth and Planetary Science Letters, 310(3-4), 293-302.
287 Fei, Y., Zhang, L., Corgne, A., Watson, H., Ricolleau, A., Meng, Y., and Prakapenka, V.
288 (2007) Spin transition and equations of state of (Mg, Fe)O solid solutions.

289 Geophysical Research Letters, 34(17).

290 Fialin, M., Catillon, G., and Andrault, D. (2008) Disproportionation of Fe^{2+} in Al-free
291 silicate perovskite in the laser heated diamond anvil cell as recorded by electron
292 probe microanalysis of oxygen. Physics and Chemistry of Minerals, 36(4),
293 183-191.

294 Frost, D.J., and McCammon, C.A. (2008) The redox state of Earth's mantle. Annual
295 Review of Earth and Planetary Sciences, 36, 389-420.

296 Frost, D.J., Liebske, C., Langenhorst, F., McCammon, C.A., Tronnes, R.G., and Rubie,
297 D.C. (2004) Experimental evidence for the existence of iron-rich metal in the
298 Earth's lower mantle. Nature, 428(6981), 409-412.

299 Fujino, K., Nishio-Hamane, D., Seto, Y., Sata, N., Nagai, T., Shinmei, T., Irifune, T.,
300 Ishii, H., Hiraoka, N., Cai, Y.Q., and Tsuei, K.-D. (2012) Spin transition of
301 ferric iron in Al-bearing Mg-perovskite up to 200 GPa and its implication for the
302 lower mantle. Earth and Planetary Science Letters, 317, 407-412.

303 Glazyrin, K., Ballaran, T.B., Frost, D.J., McCammon, C., Kantor, A., Merlini, M.,
304 Hanfland, M., and Dubrovinsky, L. (2014) Magnesium silicate perovskite and
305 effect of iron oxidation state on its bulk sound velocity at the conditions of the
306 lower mantle. Earth and Planetary Science Letters, 393, 182-186.

307 Greenberg, E., Rozenberg, G.K., Xu, W., Pasternak, M.P., McCammon, C., Glazyrin,
308 K., and Dubrovinsky, L.S. (2013) Mott transition in CaFe2O4 at around 50 GPa.
309 Physical Review B, 88, 214109.
310 Hsu, H., Umemoto, K., Blaha, P., and Wentzcovitch, R.M. (2010) Spin states and
311 hyperfine interactions of iron in (Mg,Fe)SiO_3 perovskite under pressure. Earth
312 and Planetary Science Letters, 294, 19-26.
313 Hsu, H., Blaha, P., Cococcioni, M., and Wentzcovitch, R.M. (2011) Spin-State
314 Crossover and Hyperfine Interactions of Ferric Iron in $MgSiO_3$ Perovskite.
315 Physical Review Letters, 106(11).
316 Hummer, D.R., and Fei, Y. (2012) Synthesis and crystal chemistry of Fe^{3+}-bearing
317 (Mg,Fe^{3+})(Si,Fe^{3+})O_3 perovskite. American Mineralogist, 97(11-12), 1915-1921.
318 Irifune, T., Shinmei, T., McCammon, C.A., Miyajima, N., Rubie, D.C., and Frost, D.J.
319 (2010) Iron partitioning and density changes of pyrolite in Earth's lower mantle.
320 Science 327, 193-195.
321 Jackson, J.M., Sturhahn, W., Shen, G.Y., Zhao, J.Y., Hu, M.Y., Errandonea, D., Bass,
322 J.D., and Fei, Y.W. (2005) A synchrotron Mossbauer spectroscopy study of
323 (Mg,Fe)SiO_3 perovskite up to 120 GPa. American Mineralogist, 90(1), 199-205.
324 Kaminsky, F.V., Ryabchikov, I.D., McCammon, C.A., Longo, M., Abakumov, A. M.,

325 Turner, S., and Heidari H. (2015) Oxidation potential in the Earth's lower
326 mantle as recorded by ferropericlase inclusions in diamond. Earth and Planetary
327 Science Letters, 417, 49-56.
328 Keppler, H., Dubrovinsky, L.S., Narygina, O., and Kantor, I. (2008) Optical Absorption
329 and Radiative Thermal Conductivity of Silicate Perovskite to 125 Gigapascals.
330 Science, 322(5907), 1529-1532.
331 Kudoh, Y., Prewitt, C.T., Finger, L.W., Darovskikh, A., and Ito, E. (1990) Effect of iron
332 on the crystal structure of (Mg,Fe)SiO_3 perovskite. Geophysical Research
333 Letters, 17(10), 1481-1484.
334 Kupenko, I., McCammon, C., Sinmyo, R., Prescher, C., Chumakov, A.I., Kantor, A.,
335 Rüffer, R., and Dubrovinsky, L. (2014) Electronic spin state of Fe,Al-containing
336 $MgSiO_3$ perovskite at lower mantle conditions. Lithos, 189, 167-172.
337 Kupenko, I., McCammon, C., Sinmyo, R., Cerantola, V., Potapkin, V., Chumakov, A.I.,
338 Kantor, A., Rüffer, R., and Dubrovinsky, L. (2015) Oxidation state of the lower
339 mantle: In situ observations of the iron electronic configuration in bridgmanite at
340 extreme conditions. Earth and Planetary Science Letters, 423, 78-86.
341 Li, J., Sturhahn, W., Jackson, J.M., Struzhkin, V.V., Lin, J.F., Zhao, J., Mao, H.K., and
342 Shen, G. (2006) Pressure effect on the electronic structure of iron in

(Mg,Fe)(Si,Al)O_3 perovskite: a combined synchrotron Mossbauer and X-ray emission spectroscopy study up to 100 GPa. Physics and Chemistry of Minerals, 33(8-9), 575-585.

Lin, J.-F., Watson, H., Vanko, G., Alp, E.E., Prakapenka, V.B., Dera, P., Struzhkin, V.V., Kubo, A., Zhao, J., McCammon, C., and Evans, W.J. (2008) Intermediate-spin ferrous iron in lowermost mantle post-perovskite and perovskite. Nature Geoscience, 1(10), 688-691.

Lin, J.-F., Alp, E.E., Mao, Z., Inoue, T., McCammon, C., Xiao, Y., Chow, P., and Zhao, J. (2012) Electronic spin states of ferric and ferrous iron in the lower-mantle silicate perovskite. American Mineralogist, 97(4), 592-597.

Lin, J.-F., Speziale, S., Mao, Z., and Marquardt, H. (2013) Effects of the electronic spin transitions of iron in lower mantle minerals: implications for deep mantle geophysics and geochemistry. Reviews of Geophysics, 51(2), 244-275.

Lin, J.-F., Mao, Z., Yang, J., Liu, J., Xiao, Y., Chow, P., and Okuchi T. (2016) High-spin Fe^{2+} and Fe^{3+} in single-crystal aluminous bridgmanite in the lower mantle. Geophysical Research Letters, 43(13), 6952-6959.

Lundin, S., Catalli, K., Santillan, J., Shim, S.H., Prakapenka, V.B., Kunz, M., and Meng, Y. (2008) Effect of Fe on the equation of state of mantle silicate perovskite over

1 Mbar. Physics of the Earth and Planetary Interiors, 168(1-2), 97-102.

Mao, Z., Lin, J.-F., Yang, J., Inoue, T., and Prakapenka, V.B. (2015) Effects of the Fe^{3+} spin transition on the equation of state of bridgmanite. Geophysical Research Letters, 42(11), 4335-4342.

Mashino, I., Ohtani, E., Hirao, N., Mitsui, T., Masuda, R., Seto, M., Sakai, T., Takahashi, S., and Nakano, S. (2014) The spin state of iron in Fe^{3+}-bearing Mg-perovskite and its crystal chemistry at high pressure. American Mineralogist, 99(8-9), 1555-1561.

McCammon, C. (1997) Perovskite as a possible sink for ferric iron in the lower mantle. Nature, 387(6634), 694-696.

McCammon, C.A. (2005) Mantle oxidation state and oxygen fugacity: Constraints on mantle chemistry, structure, and dynamics. In R.D. van der Hilst, J.D. Bass, J. Matas, and J. Trampert, Eds., Earth's Deep Mantle: Structure, Composition, and Evolution, p. 219-240. American Geophysical Union, Washington, D.C.

McCammon, C.A., Lauterbach, S., Seifert, F., Langenhorst, F., and van Aken, P.A. (2004) Iron oxidation state in lower mantle mineral assemblages - I. Empirical relations derived from high-pressure experiments. Earth and Planetary Science Letters, 222(2), 435-449.

McCammon, C., Kantor, I., Narygina, O., Rouquette, J., Ponkratz, U., Sergueev, I., Mezouar, M., Prakapenka, V., and Dubrovinsky, L. (2008) Stable intermediate-spin ferrous iron in lower-mantle perovskite. Nature Geoscience, 1(10), 684-687.

McCammon, C., Glazyrin, K., Kantor, A., Kantor, I., Kupenko, I., Narygina, O., Potapkin, V., Prescher, C., Sinmyo, R., Chumakov, A., Rüffer, R., Sergueev, I., Smirnov, G., and Dubrovinsky, L. (2013) Iron spin state in silicate perovskite at conditions of the Earth's deep interior. High Pressure Research, 33(3), 663-672.

Metsue, A., and Tsuchiya, T. (2012) Thermodynamic properties of $(Mg,Fe^{2+})SiO_3$ perovskite at the lower-mantle pressures and temperatures: an internally consistent LSDA+U study. Geophysical Journal International, 190(1), 310-322.

Muir, J.M.R., and Brodholt, J.P., (2015) Elastic properties of ferropericlase at lower mantle conditions and its relevance to ULVZs. Earth and Planetary Science Letters, 417, 40-48.

Nakajima, Y., Frost, D.J., and Rubie, D.C. (2012) Ferrous iron partitioning between magnesium silicate perovskite and ferropericlase and the composition of perovskite in the Earth's lower mantle. Journal of Geophysical Research-Solid Earth, 117.

Ohta, K., Hirose, K., Ichiki, M., Shimizu, K., Sata, N., and Ohishi, Y. (2010) Electrical conductivities of pyrolitic mantle and MORB materials up to the lowermost mantle conditions. Earth and Planetary Science Letters, 289(3-4), 497-502.

Ohta, K., Yagi, T., and Hirose, K. (2014) Thermal diffusivities of $MgSiO_3$ and Al-bearing $MgSiO_3$ perovskites. American Mineralogist, 99(1), 94-97.

Potapkin, V., McCammon, C., Glazyrin, K., Kantor, A., Kupenko, I., Prescher, C., Sinmyo, R., Smirnov, G.V., Chumakov, A.I., Rüffer, R., and Dubrovinsky, L. (2013) Effect of iron oxidation state on the electrical conductivity of the Earth's lower mantle. Nature Communications, 4.

Prescher, C., McCammon, C., and Dubrovinsky, L. (2012) MossA: a program for analyzing energy-domain Mossbauer spectra from conventional and synchrotron sources. Journal of Applied Crystallography, 45, 329-331.

Prescher, C., Langenhorst, F., Dubrovinsky, L.S., Prakapenka, V.B., and Miyajima, N. (2014) The effect of Fe spin crossovers on its partitioning behavior and oxidation state in a pyrolitic Earth's lower mantle system. Earth and Planetary Science Letters, 399, 86-91.

Ringwood, A.E. (1991) Phase transformations and their bearing on the constitution and dynamics of the mantle. Geochimica et Cosmochimica Acta, 55, 2083-2110.

Rozenberg, G.K., Pasternak, M.P., Xu, W.M., Dubrovinsky, L.S., Carlson, S., and Taylor, R.D. (2005) Consequences of pressure-instigated spin crossover in $RFeO_3$ perovskites; a volume collapse with no symmetry modification. Europhysics Letters, 71, 228–234.

Sinmyo, R., and Hirose K. (2010) The Soret diffusion in laser-heated diamond-anvil cell. Physics of the Earth and Planetary Interiors, 180, 172-178.

Sinmyo, R., and Hirose, K. (2013) Iron partitioning in pyrolitic lower mantle. Physics and Chemistry of Minerals, 40(2), 107-113.

Sinmyo, R., Ozawa, H., Hirose, K., Yasuhara, A., Endo, N., Sata, N., and Ohishi, Y. (2008) Ferric iron content in $(Mg,Fe)SiO_3$ perovskite and post-perovskite at deep lower mantle conditions. American Mineralogist, 93(11-12), 1899-1902.

Sinmyo, R., Hirose, K., Muto, S., Ohishi, Y., and Yasuhara, A. (2011) The valence state and partitioning of iron in the Earth's lowermost mantle. Journal of Geophysical Research-Solid Earth, 116.

Sinmyo, R., Pesce, G., Greenberg, E., McCammon, C., and Dubrovinsky, L. (2014a) Lower mantle electrical conductivity based on measurements of Al, Fe-bearing perovskite under lower mantle conditions. Earth and Planetary Science Letters, 393, 165-172.

433 Sinmyo, R., Bykova, E., McCammon, C., Kupenko, I., Potapkin, V., and Dubrovinsky,
434 L. (2014b) Crystal chemistry of Fe^{3+}-bearing (Mg, Fe)SiO_3 perovskite: a
435 single-crystal X-ray diffraction study. Physics and Chemistry of Minerals, 41(6),
436 409-417.
437 Stagno, V., Ojwang, D.O., McCammon, C.A., and Frost, D.J. (2013) The oxidation
438 state of the mantle and the extraction of carbon from Earth's interior. Nature,
439 493, 84-88.
440 Umemoto, K., Wentzcovitch, R.M., Yu, Y.G., and Requist, R. (2008) Spin transition in
441 (Mg,Fe)SiO_3 perovskite under pressure. Earth and Planetary Science Letters,
442 276(1-2), 198-206.
443 Vanpeteghem, C.B., Angel, R.J., Ross, N.L., Jacobsen, S.D., Dobson, D.P., Litasov,
444 K.D., and Ohtani, E. (2006) Al, Fe substitution in the $MgSiO_3$ perovskite
445 structure: A single-crystal X-ray diffraction study. Physics of the Earth and
446 Planetary Interiors, 155(1-2), 96-103.
447 Vilella, K., Shim, S.H., Farnetani, C.G., Badro, J., (2015) Spin state transition and
448 partitioning of iron: Effects on mantle dynamics. Earth and Planetary Science
449 Letters, 417, 57-66.
450 Wang, X., Tsuchiya, T., and Hase, A. (2015) Computational support for a pyrolitic

lower mantle containing ferric iron. Nature Geoscience, 8(7), 556-559.

Wentzcovitch, R.M., Justo, J.F., Wu, Z., da Silva, C.R.S., Yuen, D.A., and Kohlstedt, D. (2009) Anomalous compressibility of ferropericlase throughout the iron spin cross-over. Proceedings of the National Academy of Sciences of the United States of America, 106(21), 8447-8452.

Wolf, A.S., Jackson, J.M., Dera, P., and Prakapenka, V.B. (2015) The thermal equation of state of (Mg, Fe)SiO_3 bridgmanite (perovskite) and implications for lower mantle structures. Journal of Geophysical Research-Solid Earth, 120

Xu, W., Greenberg, E., Rozenberg, G.K., Pasternak, M.P., Bykova, E., Boffa-Ballaran, T., Dubrovinsky, L., Prakapenka, V., Hanfland, M., Vekilova, O.Y., Simak, S.I., and Abrikosov, I.A. (2013) Pressure-induced hydrogen bond symmetrization in iron oxyhydroxide. Physical Review Letters 111, 175501.

Yoshino, T., Ito, E., Katsura, T., Yamazaki, D., Shan, S., Guo, X., Nishi, M., Higo, Y., and Funakoshi, K. (2011) Effect of iron content on electrical conductivity of ferropericlase with implications for the spin transition pressure. Journal of Geophysical Research-Solid Earth, 116.

Yoshino, T., Kamada, S., Zhao, C., Ohtani, E., Hirao, N. (2016) Electrical conductivity model of Al-bearing bridgmanite with implications for the electrical structure of

the Earth's lower mantle. Earth and Planetary Science Letters, 434, 208-219.

Figure captions

Figure 1. Selected Mössbauer spectra of Al-free Fe^{3+}-rich Bdg at different pressures and room temperature. Experimental data are indicated by solid circles while the fitted curve is shown by the thick solid line. Components are shaded as indicated in part (c) and the fitting residual is shown beneath each spectrum.

Figure 2. Pressure dependence of center shift (CS) and quadrupole splitting (QS) for (a) Fe^{2+} and (b) Fe^{3+} in Al-free Bdg. Right and left pointing triangles indicate data taken during compression and decompression, respectively. Our results are largely consistent with previously reported values for Al-free Bdg (Potapkin et al. 2013).

Figure 3. Relative abundance of components fitted to Mössbauer spectra of Al-free Bdg: (a) Fe^{2+} ; (b) Fe^{3+}. The dashed line shows the initial abundance of Fe^{2+} and Fe^{3+}.

Figure 4. Variation of CS and QS values for Bdg. Circles, this study; squares, Al-free Bdg at ambient conditions (Hummer and Fei 2012); diamonds, Al-bearing Bdg under 12

487 - 77 GPa (Kupenko et al. 2015). The diameters of the circles are proportional to the
488 pressure at which the values were obtained (i.e., larger diameters correspond to higher
489 pressures).
490
491 Figure 5. Relation between Fe^{3+} concentration (in cations per formula unit) and the
492 saturation pressure of low-spin Fe^{3+} in Bdg (see text for details). The grey line is an
493 empirical fit to the data for Bdg samples synthesized using a large volume press where
494 $Fe^{3+}/\Sigma Fe$ ratios were experimentally determined. Red symbols, Al-free Bdg; blue
495 symbols, Al-bearing Bdg. Filled symbols indicate the data used for fitting (Color
496 online). "Harzburgite", "Pyrolite" and "MORB" denote possible concentrations of Fe^{3+}
497 in Bdg in harzburgitic, pyrolitic and basaltic rock, respectively (see text for details).

This is a preprint, the final version is subject to change, of the American Mineralogist (MSA)
Cite as Authors (Year) Title. American Mineralogist, in press.
(DOI will not work until issue is live.) DOI: http://dx.doi.org/10.2138/am-2017-5917

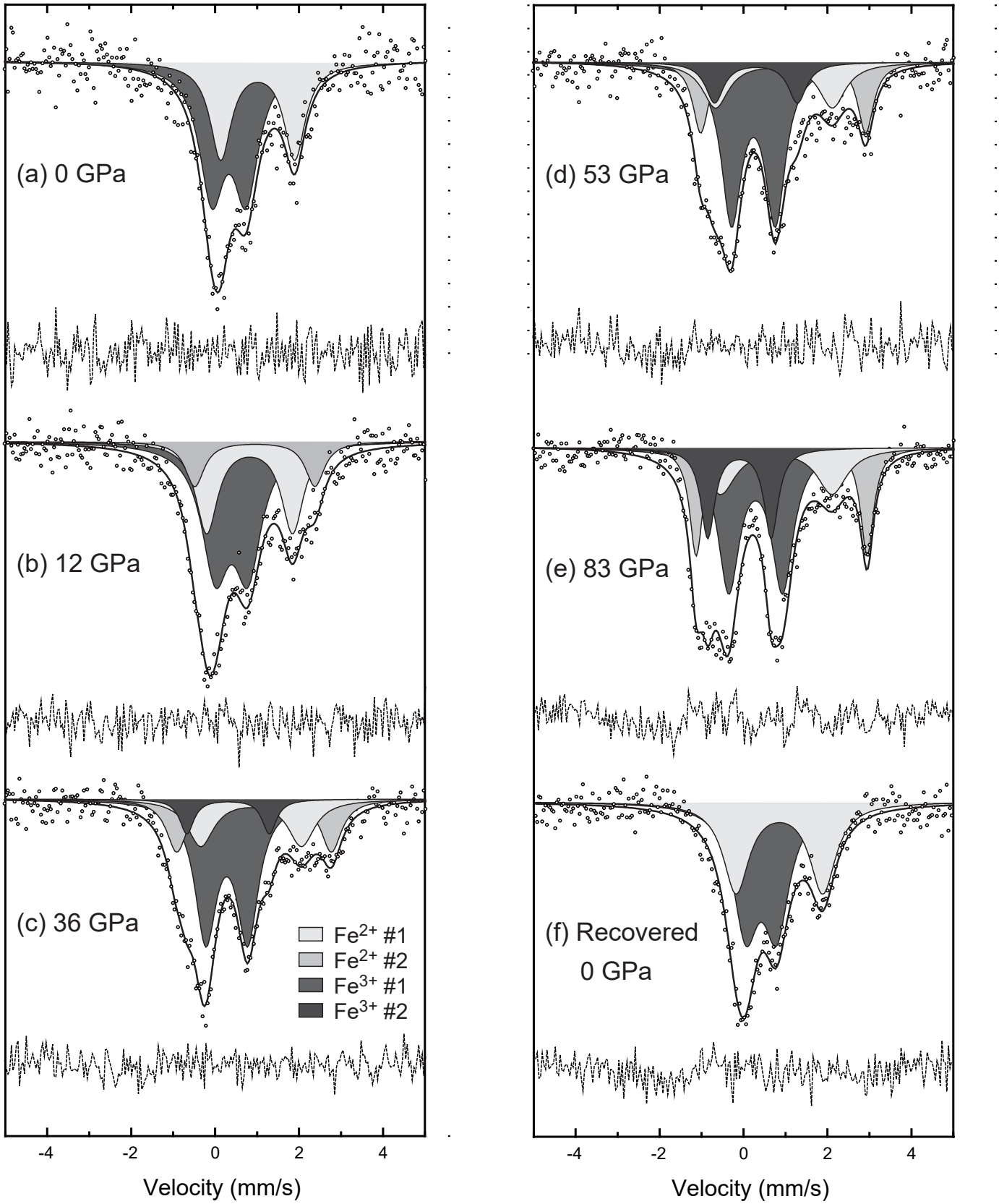

Figure 1

This is a preprint, the final version is subject to change, of the American Mineralogist (MSA)
Cite as Authors (Year) Title. American Mineralogist, in press.
(DOI will not work until issue is live.) DOI: http://dx.doi.org/10.2138/am-2017-5917

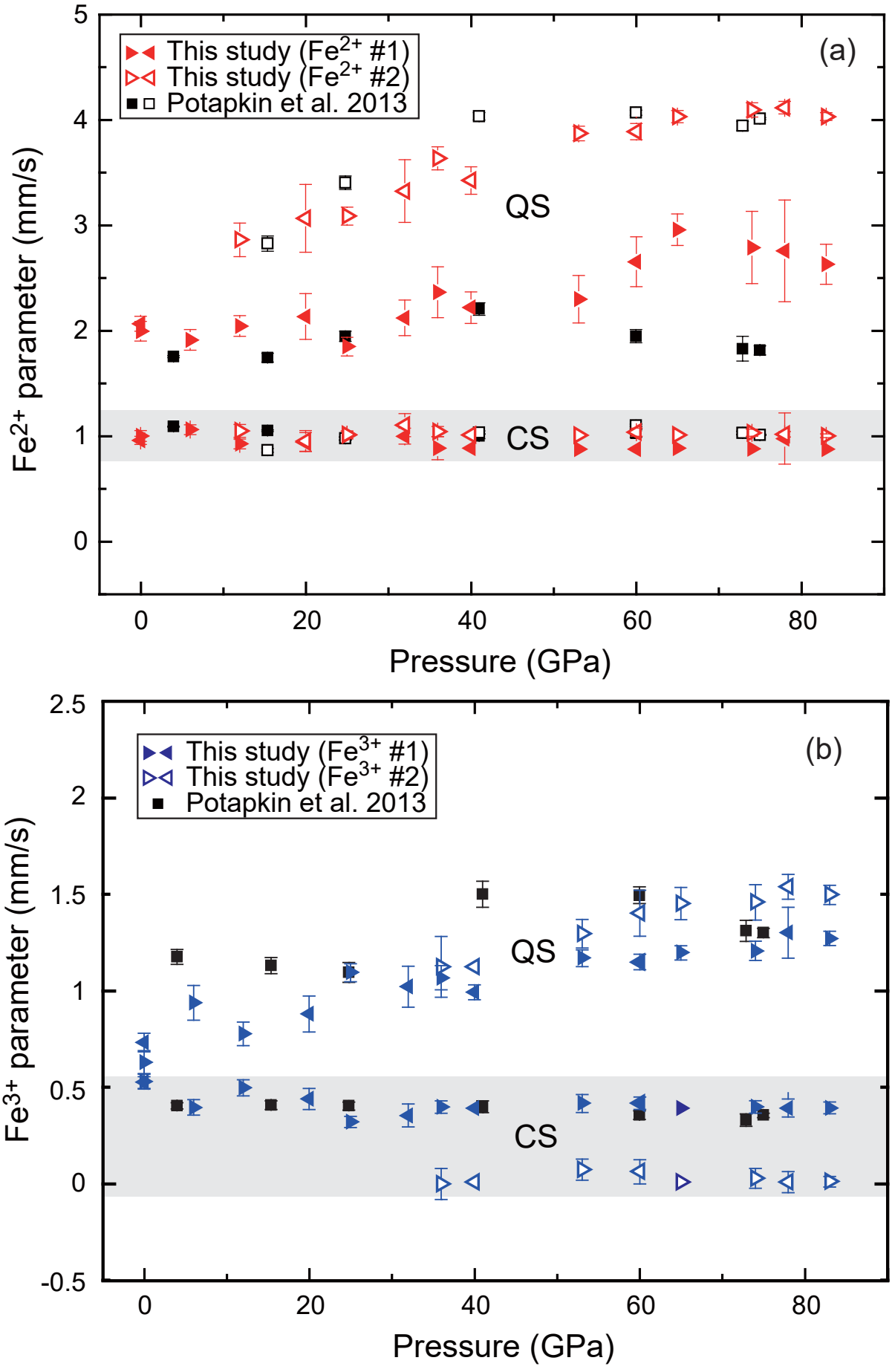

Figure 2

This is a preprint, the final version is subject to change, of the American Mineralogist (MSA)
Cite as Authors (Year) Title. American Mineralogist, in press.
(DOI will not work until issue is live.) DOI: http://dx.doi.org/10.2138/am-2017-5917

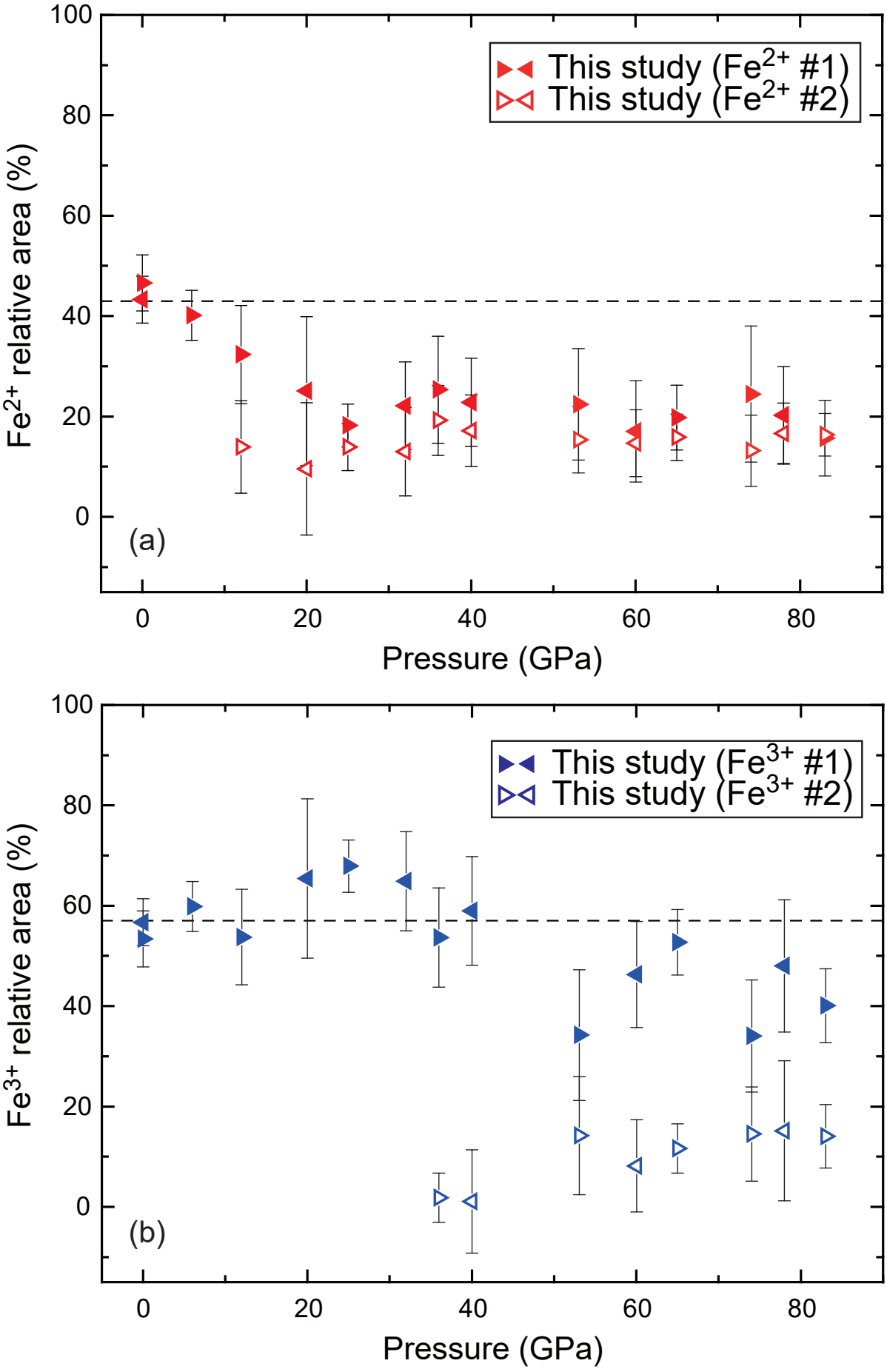

Figure 3

This is a preprint, the final version is subject to change, of the American Mineralogist (MSA)
Cite as Authors (Year) Title. American Mineralogist, in press.
(DOI will not work until issue is live.) DOI: http://dx.doi.org/10.2138/am-2017-5917

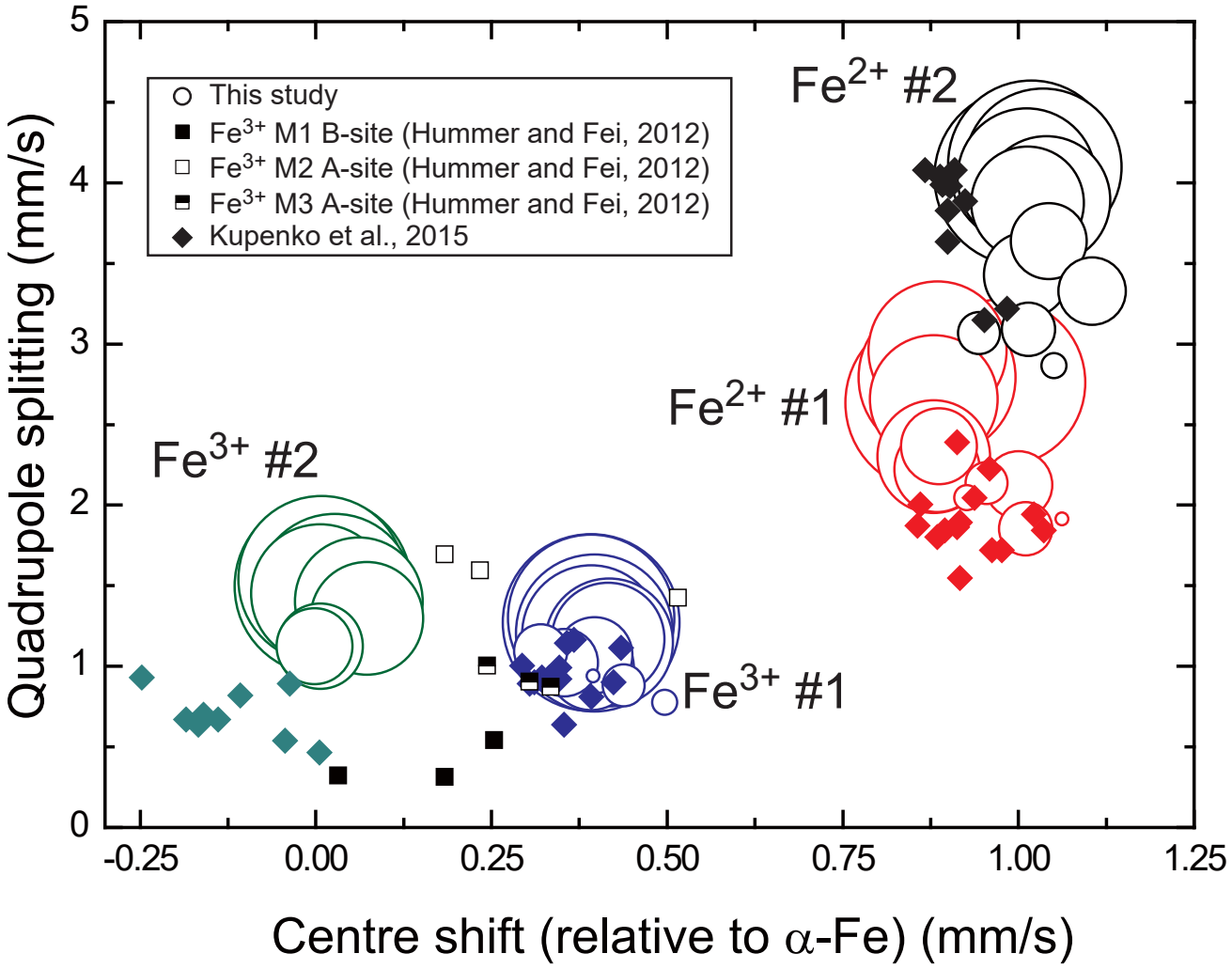

Figure 4

This is a preprint, the final version is subject to change, of the American Mineralogist (MSA)
Cite as Authors (Year) Title. American Mineralogist, in press.
(DOI will not work until issue is live.) DOI: http://dx.doi.org/10.2138/am-2017-5917

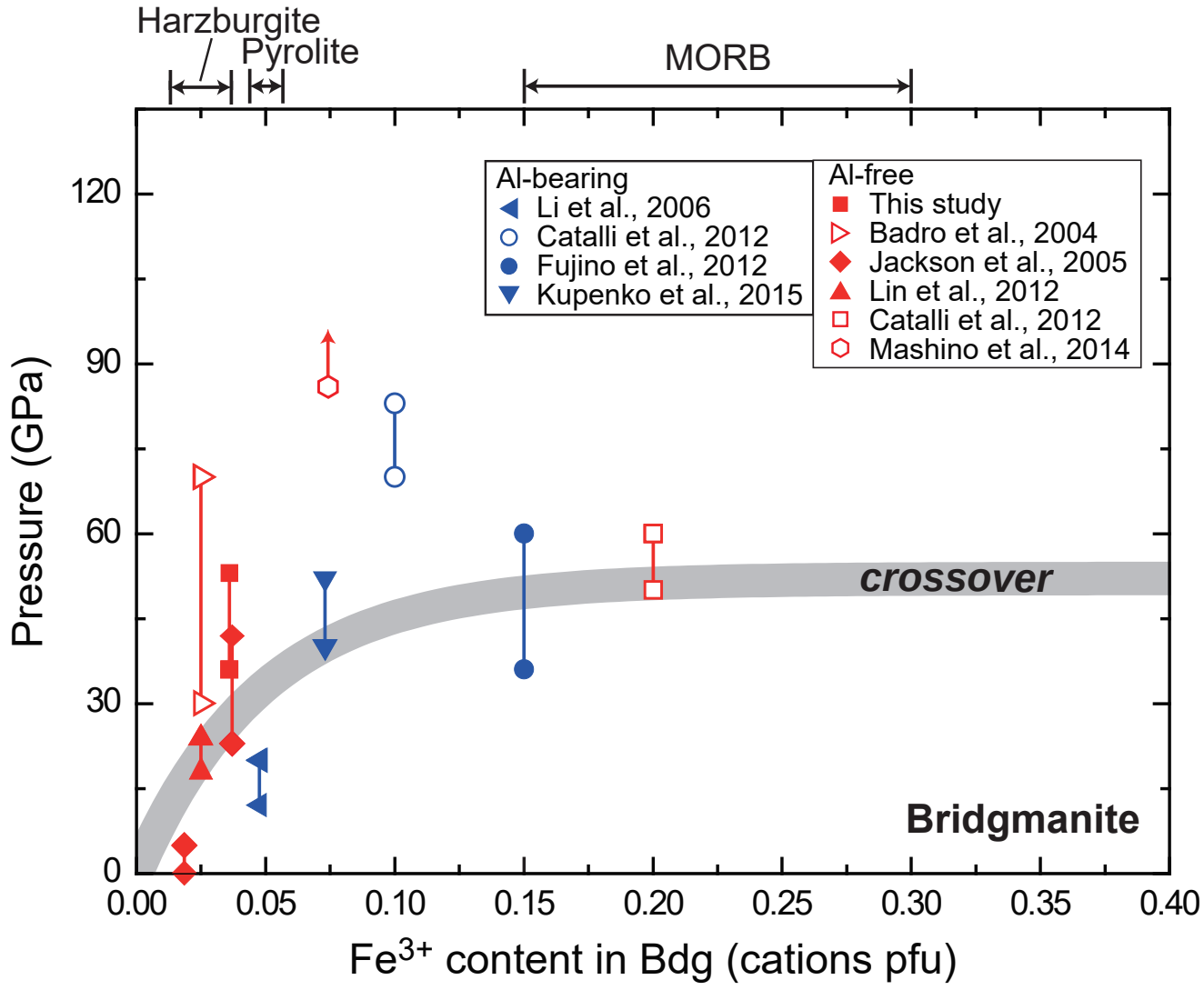

Figure 5

This is a preprint, the final version is subject to change, of the American Mineralogist (MSA)
Cite as Authors (Year) Title. American Mineralogist, in press.
(DOI will not work until issue is live.) DOI: http://dx.doi.org/10.2138/am-2017-5917

Table 1. Hyperfine parameters of Fe^{3+}-rich bridgmanite determined from room temperature Mössbauer spectra.

Pressure (GPa)	Component	CS (mm/s)	FWHM (mm/s)	Area (%)	QS (mm/s)	Fe^{3+}/total Fe (%)
Compression						
0	Fe^{2+} #1	1.00(5)	0.75(15)	47(6)	2.00(9)	53
	Fe^{3+} #1	0.53(4)	0.66(13)	53(6)	0.63(6)	
6	Fe^{2+} #1	1.06(5)	0.77(13)	40(5)	1.91(10)	60
	Fe^{3+} #1	0.40(4)	0.92(13)	60(5)	0.94(9)	
12	Fe^{2+} #1	0.93(5)	0.64(21)	32(10)	2.05(10)	54
	Fe^{2+} #2	1.05(6)	0.55(26)	14(9)	2.86(16)	
	Fe^{3+} #1	0.50(4)	0.79(13)	54(10)	0.78(6)	
25	Fe^{2+} #1	1.01(4)	0.46(15)	14(5)	1.85(9)	68
	Fe^{2+} #2	1.01(4)	0.54(13)	18(4)	3.09(9)	
	Fe^{3+} #1	0.32(3)	0.95(11)	68(5)	1.09(5)	
36	Fe^{2+} #1	0.89(11)	0.92(42)	25(11)	2.36(24)	55
	Fe^{2+} #2	1.04(5)	0.61(19)	19(7)	3.64(11)	
	Fe^{3+} #1	0.40(3)	0.67(11)	54(10)	1.07(6)	
	Fe^{3+} #2	0.00(8)	0.19(41)	2(5)	1.12(16)	
53	Fe^{2+} #1	*0.88*	0.93(40)	26(11)	2.30(22)	54
	Fe^{2+} #2	*1.01*	0.47(12)	19(6)	3.87(7)	
	Fe^{3+} #1	0.42(5)	0.56(16)	37(12)	1.17(4)	
	Fe^{3+} #2	0.07(6)	0.45(18)	18(11)	1.29(7)	
65	Fe^{2+} #1	*0.88*	0.67(27)	20(6)	2.96(15)	64
	Fe^{2+} #2	*1.01*	0.37(10)	16(5)	4.03(6)	
	Fe^{3+} #1	*0.39*	0.63(7)	53(7)	1.20(4)	
	Fe^{3+} #2	*0.01*	0.37(15)	12(5)	1.45(8)	
74	Fe^{2+} #1	*0.88*	1.06(60)	28(13)	2.79(34)	55
	Fe^{2+} #2	1.04(3)	0.37(13)	17(7)	4.10(7)	
	Fe^{3+} #1	0.40(3)	0.50(12)	37(11)	1.21(5)	
	Fe^{3+} #2	0.03(5)	0.43(17)	18(9)	1.46(9)	
83	Fe^{2+} #1	*0.88*	0.85(38)	19(7)	2.63(19)	61
	Fe^{2+} #2	1.01(2)	0.37(6)	20(4)	4.03(4)	
	Fe^{3+} #1	0.39(3)	0.62(9)	43(7)	1.27(4)	
	Fe^{3+} #2	0.01(3)	0.40(10)	18(6)	1.50(5)	
Decompression						
78	Fe^{2+} #1	0.98(24)	0.77(41)	20(10)	2.76(48)	63
	Fe^{2+} #2	1.02(3)	0.38(10)	17(6)	4.12(6)	
	Fe^{3+} #1	0.39(5)	0.70(12)	48(13)	1.30(13)	
	Fe^{3+} #2	0.01(6)	0.37(21)	15(14)	1.54(6)	
60	Fe^{2+} #1	*0.88*	0.82(38)	20(12)	2.56(78)	62
	Fe^{2+} #2	1.04(4)	0.37(6)	18(9)	3.94(8)	
	Fe^{3+} #1	0.42(3)	0.62(9)	44(21)	1.19(15)	
	Fe^{3+} #2	0.06(6)	0.40(10)	18(24)	1.43(9)	
40	Fe^{2+} #1	*0.88*	0.68(27)	23(9)	2.22(15)	60
	Fe^{2+} #2	*1.01*	0.56(21)	17(7)	3.43(13)	
	Fe^{3+} #1	*0.39*	0.65(10)	59(11)	0.99(4)	
	Fe^{3+} #2	*0.01*	0.64(456)	1(10)	*1.12*	
32	Fe^{2+} #1	1.00(8)	0.53(23)	22(9)	2.12(17)	65
	Fe^{2+} #2	1.10(11)	0.65(45)	13(9)	3.33(30)	
	Fe^{3+} #1	0.35(6)	0.85(16)	65(10)	1.02(11)	
20	Fe^{2+} #1	0.95(10)	0.61(37)	25(15)	2.14(22	65
	Fe^{2+} #2	0.94(9)	0.49(48)	10(13)	3.07(32)	
	Fe^{3+} #1	0.44(6)	0.74(12)	65(16)	0.88(9)	
0	Fe^{2+} #1	0.96(4)	0.75(12)	43(5)	2.07(7)	57
	Fe^{3+} #1	0.53(3)	0.74(11)	57(5)	0.73(5)	

Values in italics were held fixed during fitting